Reconstruction of sparse scatterers through a Bayesian Compressive Sampling-based Inversion Technique under the Rytov Approximations

L. Poli, G. Oliveri, P. Rocca, A. Massa

Abstract

This report proposes the numerical validation of a Bayesian Compressive Sensing technique applied to solve an inverse scattering problem within the Rytov approximation. The reconstruction of sparse objects has been investigated, considering single or multiple objects with different shape and different values of dielectric permittivity.

Contents

1 Numerical Validation within Sparsity Conditions

1.1 TEST CASE: Four Square Cylinders $L = 0.16\lambda$

Goal: show the performances of BCS when dealing with a sparse scatterer

- Number of Views: V
- Number of Measurements: M
- Number of Cells for the Inversion: N
- Number of Cells for the Direct solver: D
- Side of the investigation domain: L

Test Case Description

Direct solver:

- Square domain divided in $\sqrt{D} \times \sqrt{D}$ cells
- Domain side: $L = 3\lambda$
- $D = 1296$ (discretization for the direct solver: $< \lambda/10$)

Investigation domain:

- Square domain divided in $\sqrt{N} \times \sqrt{N}$ cells
- $L = 3\lambda$
- $2ka = 2 \times \frac{2\pi}{\lambda} \times \frac{L\sqrt{2}}{2} = 6\pi\sqrt{2} = 26.65$
- $\#DOF = \frac{(2ka)^2}{2} = \frac{(2\times\frac{2\pi}{\lambda}\times\frac{L\sqrt{2}}{2})^2}{2} = 4\pi^2\left(\frac{L}{\lambda}\right)^2 = 4\pi^2 \times 9 \approx 355.3$
- N scelto in modo da essere vicino a $\#DOF$: $N = 324$ (18×18)

Measurement domain:

- Measurement points taken on a circle of radius $\rho = 3\lambda$
- Full-aspect measurements
- $M \approx 2ka \rightarrow M = 27$

Sources:

- Plane waves
- $V \approx 2ka \rightarrow V = 27$
- Amplitude: $A = 1$
- Frequency: 300 MHz $(\lambda = 1)$

Object:

- Two square cylinders of side $\frac{\lambda}{6} = 0.1667$
- $\varepsilon_r \in \{1.5, 2.0, 2.5, 3.0\}$ (two square), $\varepsilon_r = 1.9$ (two square)

- $\sigma = 0$ [S/m]

BCS parameters:

- Initial estimate of the noise: $n_0 = 8.0 \times 10^{-3}$
- Convergenze parameter: $\tau = 1.0 \times 10^{-8}$

RESULTS: Four Square Cylinders $L = 0.16\lambda$

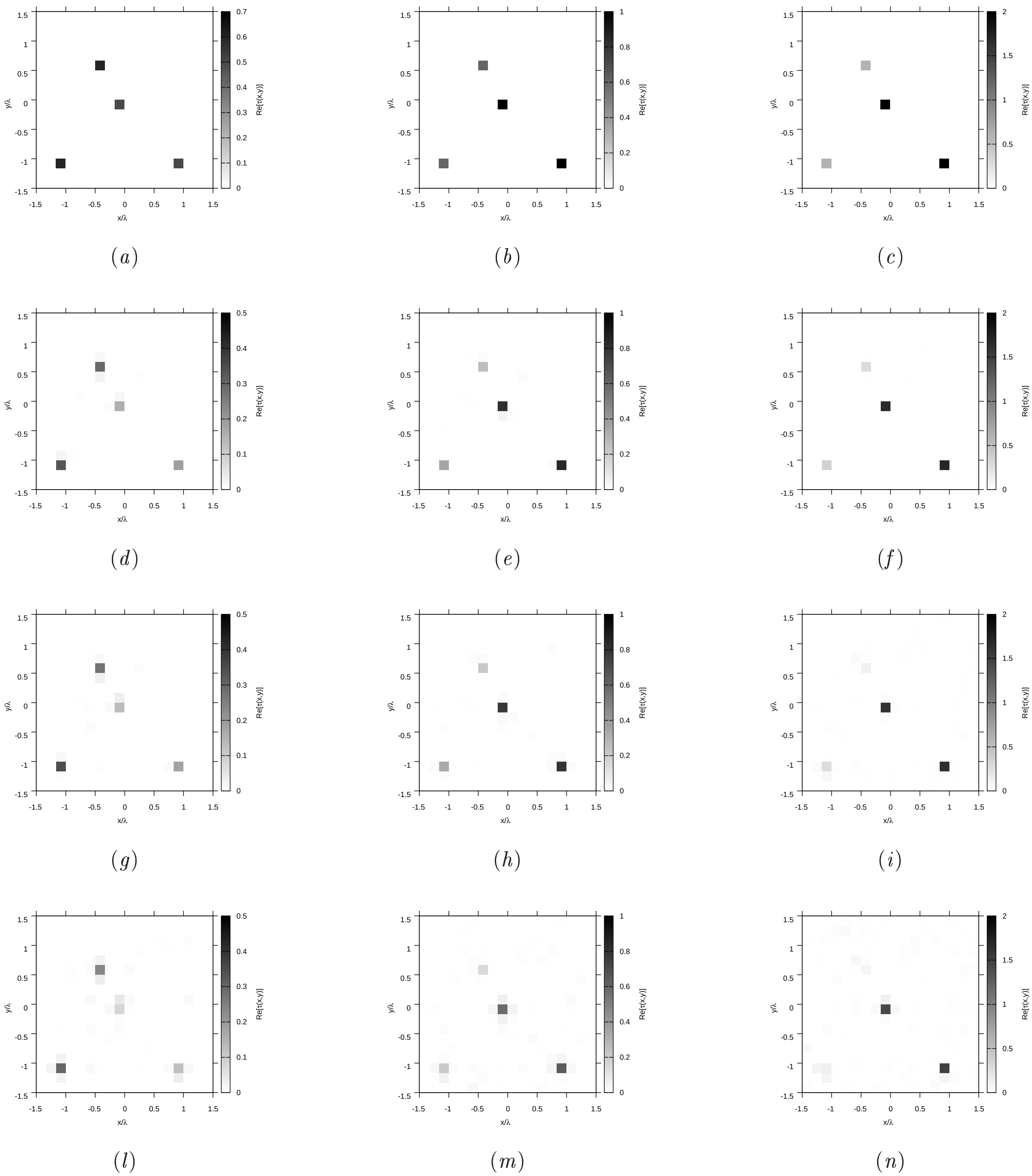

Figure 1. Actual object $(a)(b)(c)$ and BCS reconstructed object with $(d)(g)(l)$ $\varepsilon_r = 1.5$, $(e)(h)(m)$ $\varepsilon_r = 2.0$, and $(f)(i)(n)$ $\varepsilon_r = 3.0$, for $(d)(e)(f)$ Noiseless case, $(g)(h)(i)$ $SNR = 10$ [dB] and $(l)(m)(n)$ $SNR = 5$ [dB].

RESULTS: Two Square Cylinders $L = 0.16\lambda$ - Error Figures - Comparison Born/Rytov Approximation

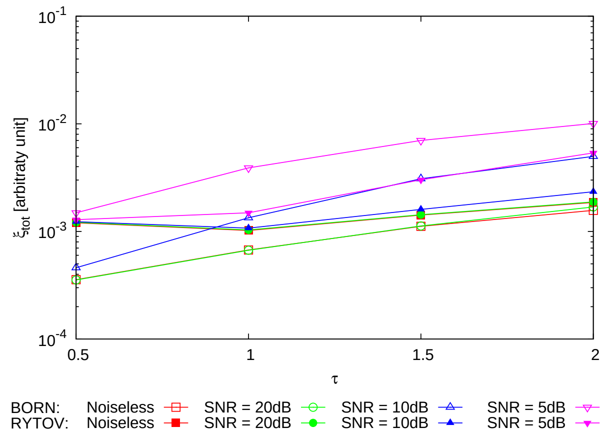

(a)

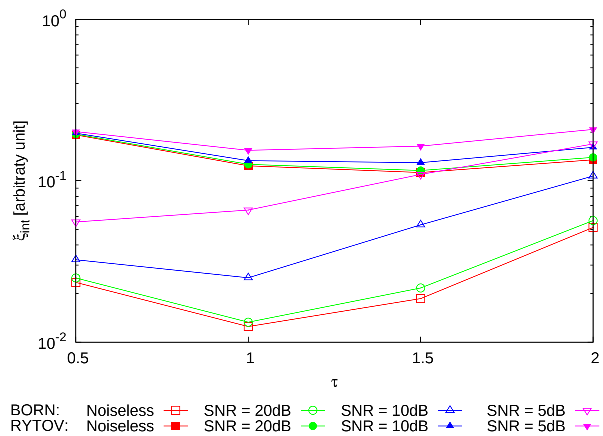

(b)

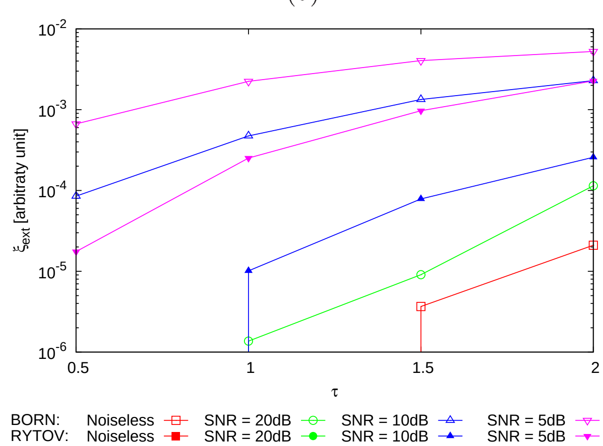

(c)

Figure 2. Behaviour of error figures as a function of ε_r, for different SNR values: (a) total error ξ_{tot}, (b) internal error ξ_{int}, (c) external error ξ_{ext}.

1.2 TEST CASE: Cross-Shaped Cylinder

Goal: show the performances of BCS when dealing with a sparse scatterer

- Number of Views: V
- Number of Measurements: M
- Number of Cells for the Inversion: N
- Number of Cells for the Direct solver: D
- Side of the investigation domain: L

Test Case Description

Direct solver:

- Square domain divided in $\sqrt{D} \times \sqrt{D}$ cells
- Domain side: $L = 3\lambda$
- $D = 1296$ (discretization for the direct solver: $< \lambda/10$)

Investigation domain:

- Square domain divided in $\sqrt{N} \times \sqrt{N}$ cells
- $L = 3\lambda$
- $2ka = 2 \times \frac{2\pi}{\lambda} \times \frac{L\sqrt{2}}{2} = 6\pi\sqrt{2} = 26.65$
- $\#DOF = \frac{(2ka)^2}{2} = \frac{(2\times\frac{2\pi}{\lambda}\times\frac{L\sqrt{2}}{2})^2}{2} = 4\pi^2\left(\frac{L}{\lambda}\right)^2 = 4\pi^2 \times 9 \approx 355.3$
- N scelto in modo da essere vicino a $\#DOF$: $N = 324$ (18×18)

Measurement domain:

- Measurement points taken on a circle of radius $\rho = 3\lambda$
- Full-aspect measurements
- $M \approx 2ka \rightarrow M = 27$

Sources:

- Plane waves
- $V \approx 2ka \rightarrow V = 27$
- Amplitude: $A = 1$
- Frequency: 300 MHz ($\lambda = 1$)

Object:

- Cross-shaped cylinder
- $\varepsilon_r \in \{1.5, 2.0, 2.5, 3.0\}$
- $\sigma = 0$ [S/m]

BCS parameters:

- Initial estimate of the noise: $n_0 = 8.0 \times 10^{-3}$
- Convergenze parameter: $\tau = 1.0 \times 10^{-8}$

RESULTS: Cross-Shaped Cylinder

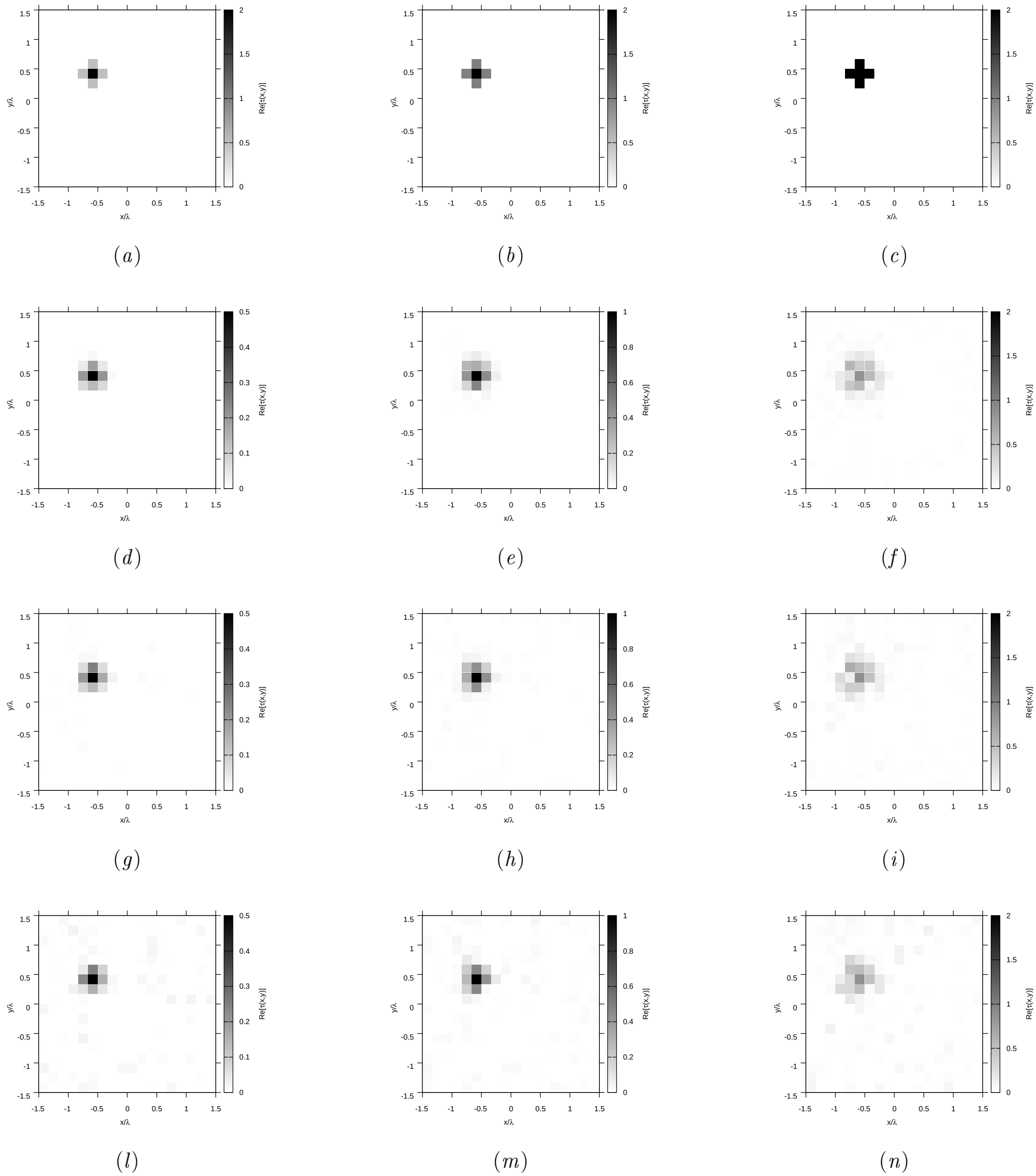

Figure 3. Actual object $(a)(b)(c)$ and BCS reconstructed object with $(d)(g)(l)$ $\varepsilon_r = 1.5$, $(e)(h)(m)$ $\varepsilon_r = 2.0$, and $(f)(i)(n)$ $\varepsilon_r = 3.0$, for $(d)(e)(f)$ Noiseless case, $(g)(h)(i)$ $SNR = 10$ [dB] and $(l)(m)(n)$ $SNR = 5$ [dB].

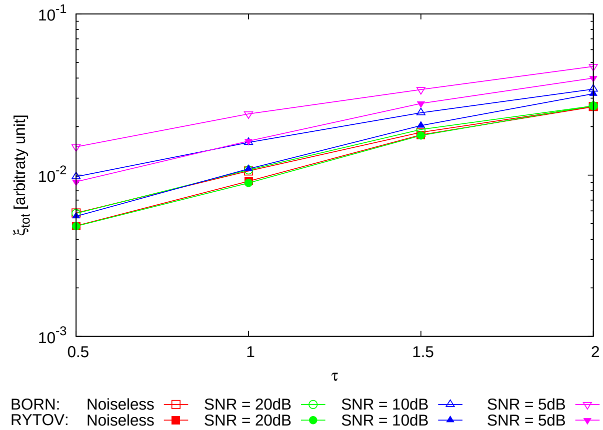

(a)

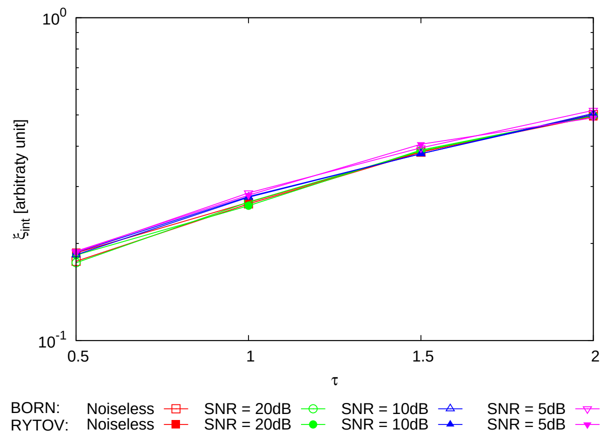

(b)

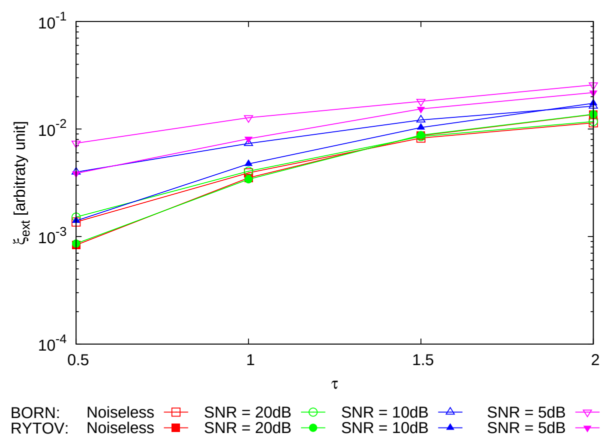

(c)

Figure 4. Behaviour of error figures as a function of ε_r, for different SNR values: (a) total error ξ_{tot}, (b) internal error ξ_{int}, (c) external error ξ_{ext}.

1.3 TEST CASE: L-Shaped Cylinder

Goal: show the performances of BCS when dealing with a sparse scatterer

- Number of Views: V
- Number of Measurements: M
- Number of Cells for the Inversion: N
- Number of Cells for the Direct solver: D
- Side of the investigation domain: L

Test Case Description

Direct solver:

- Square domain divided in $\sqrt{D} \times \sqrt{D}$ cells
- Domain side: $L = 3\lambda$
- $D = 1296$ (discretization for the direct solver: $< \lambda/10$)

Investigation domain:

- Square domain divided in $\sqrt{N} \times \sqrt{N}$ cells
- $L = 3\lambda$
- $2ka = 2 \times \frac{2\pi}{\lambda} \times \frac{L\sqrt{2}}{2} = 6\pi\sqrt{2} = 26.65$
- $\#DOF = \frac{(2ka)^2}{2} = \frac{(2\times\frac{2\pi}{\lambda}\times\frac{L\sqrt{2}}{2})^2}{2} = 4\pi^2\left(\frac{L}{\lambda}\right)^2 = 4\pi^2 \times 9 \approx 355.3$
- N scelto in modo da essere vicino a $\#DOF$: $N = 324$ (18×18)

Measurement domain:

- Measurement points taken on a circle of radius $\rho = 3\lambda$
- Full-aspect measurements
- $M \approx 2ka \rightarrow M = 27$

Sources:

- Plane waves
- $V \approx 2ka \rightarrow V = 27$
- Amplitude $A = 1$
- Frequency: 300 MHz ($\lambda = 1$)

Object:

- L-shaped cylinder
- $\varepsilon_r \in \{1.5, 2.0, 2.5, 3.0\}$
- $\sigma = 0$ [S/m]

BCS parameters:

- Initial estimate of the noise: $n_0 = 8.0 \times 10^{-3}$
- Convergenze parameter: $\tau = 1.0 \times 10^{-8}$

RESULTS: L-Shaped Cylinder

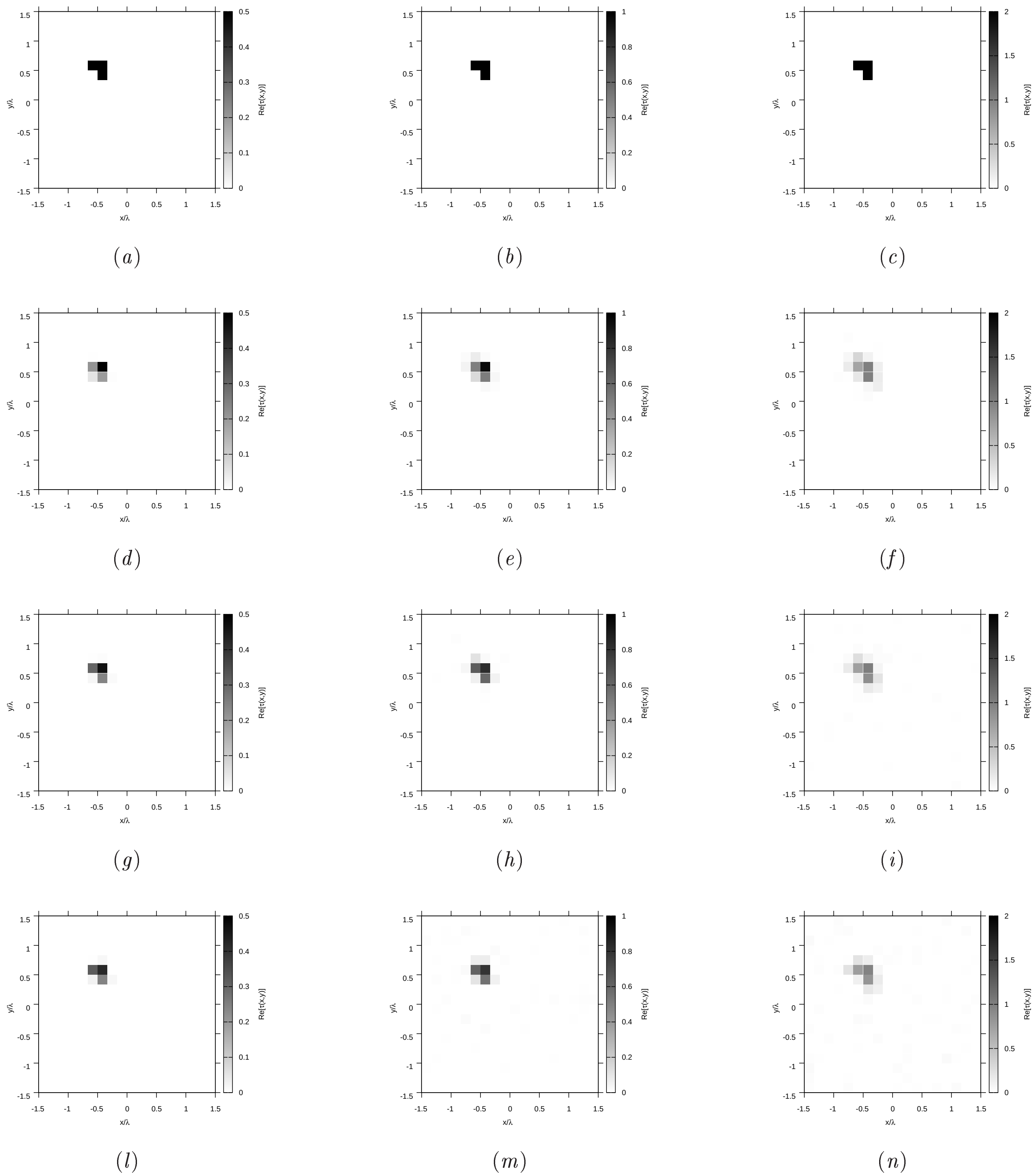

Figure 5. Actual object $(a)(b)(c)$ and BCS reconstructed object with $(d)(g)(l)$ $\varepsilon_r = 1.5$, $(e)(h)(m)$ $\varepsilon_r = 2.0$, and $(f)(i)(n)$ $\varepsilon_r = 3.0$, for $(d)(e)(f)$ Noiseless case, $(g)(h)(i)$ $SNR = 10$ [dB] and $(l)(m)(n)$ $SNR = 5$ [dB].

RESULTS: L-Shaped Cylinder - Error Figures - Comparison Born/Rytov Approximation

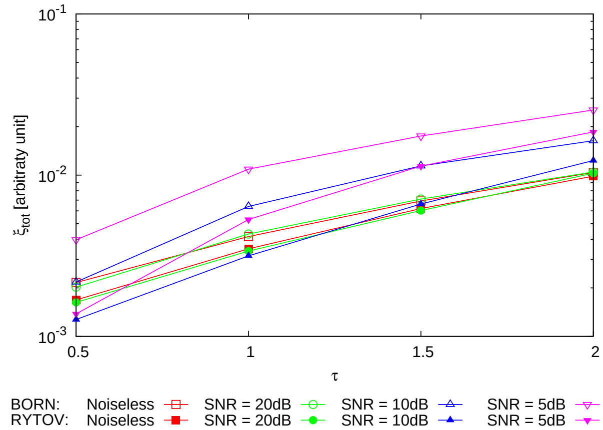

(a)

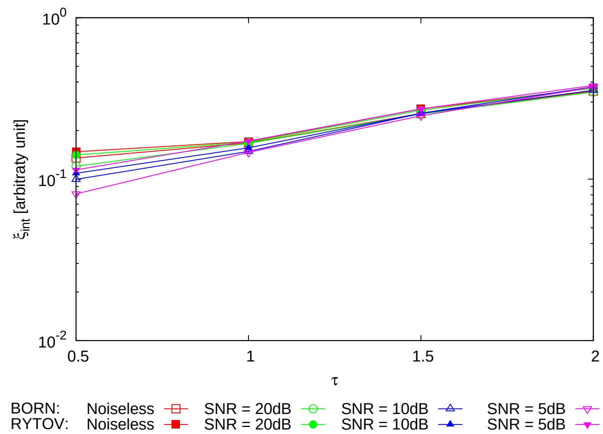

(b)

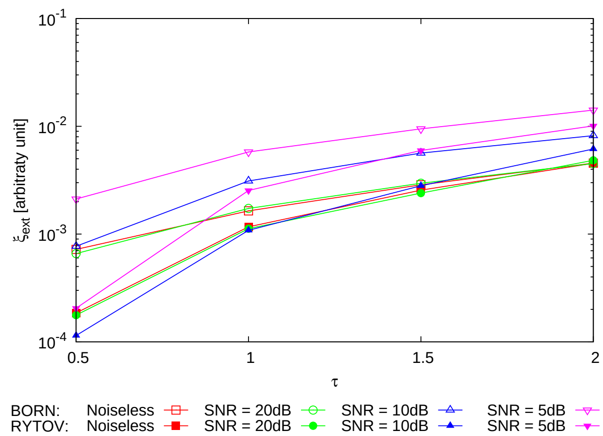

(c)

Figure 6. Behaviour of error figures as a function of ε_r, for different SNR values: (a) total error ξ_{tot}, (b) internal error ξ_{int}, (c) external error ξ_{ext}.

1.4 TEST CASE: Inhomogeneous L-Shaped Cylinder

Goal: show the performances of BCS when dealing with a sparse scatterer

- Number of Views: V
- Number of Measurements: M
- Number of Cells for the Inversion: N
- Number of Cells for the Direct solver: D
- Side of the investigation domain: L

Test Case Description

Direct solver:

- Square domain divided in $\sqrt{D} \times \sqrt{D}$ cells
- Domain side: $L = 3\lambda$
- $D = 1296$ (discretization for the direct solver: $< \lambda/10$)

Investigation domain:

- Square domain divided in $\sqrt{N} \times \sqrt{N}$ cells
- $L = 3\lambda$
- $2ka = 2 \times \frac{2\pi}{\lambda} \times \frac{L\sqrt{2}}{2} = 6\pi\sqrt{2} = 26.65$
- $\#DOF = \frac{(2ka)^2}{2} = \frac{(2\times\frac{2\pi}{\lambda}\times\frac{L\sqrt{2}}{2})^2}{2} = 4\pi^2\left(\frac{L}{\lambda}\right)^2 = 4\pi^2 \times 9 \approx 355.3$
- N scelto in modo da essere vicino a $\#DOF$: $N = 324$ (18×18)

Measurement domain:

- Measurement points taken on a circle of radius $\rho = 3\lambda$
- Full-aspect measurements
- $M \approx 2ka \rightarrow M = 27$

Sources:

- Plane waves
- $V \approx 2ka \rightarrow V = 27$
- Amplitude $A = 1$
- Frequency: 300 MHz ($\lambda = 1$)

Object:

- Inhomogeneous L-shaped cylinder
- $\varepsilon_r \in \{1.5, 2.0, 2.5, 3.0\}$
- $\sigma = 0$ [S/m]

BCS parameters:

- Initial estimate of the noise: $n_0 = 8.0 \times 10^{-3}$
- Convergenze parameter: $\tau = 1.0 \times 10^{-8}$

RESULTS: Inhomogeneous L-Shaped Cylinder

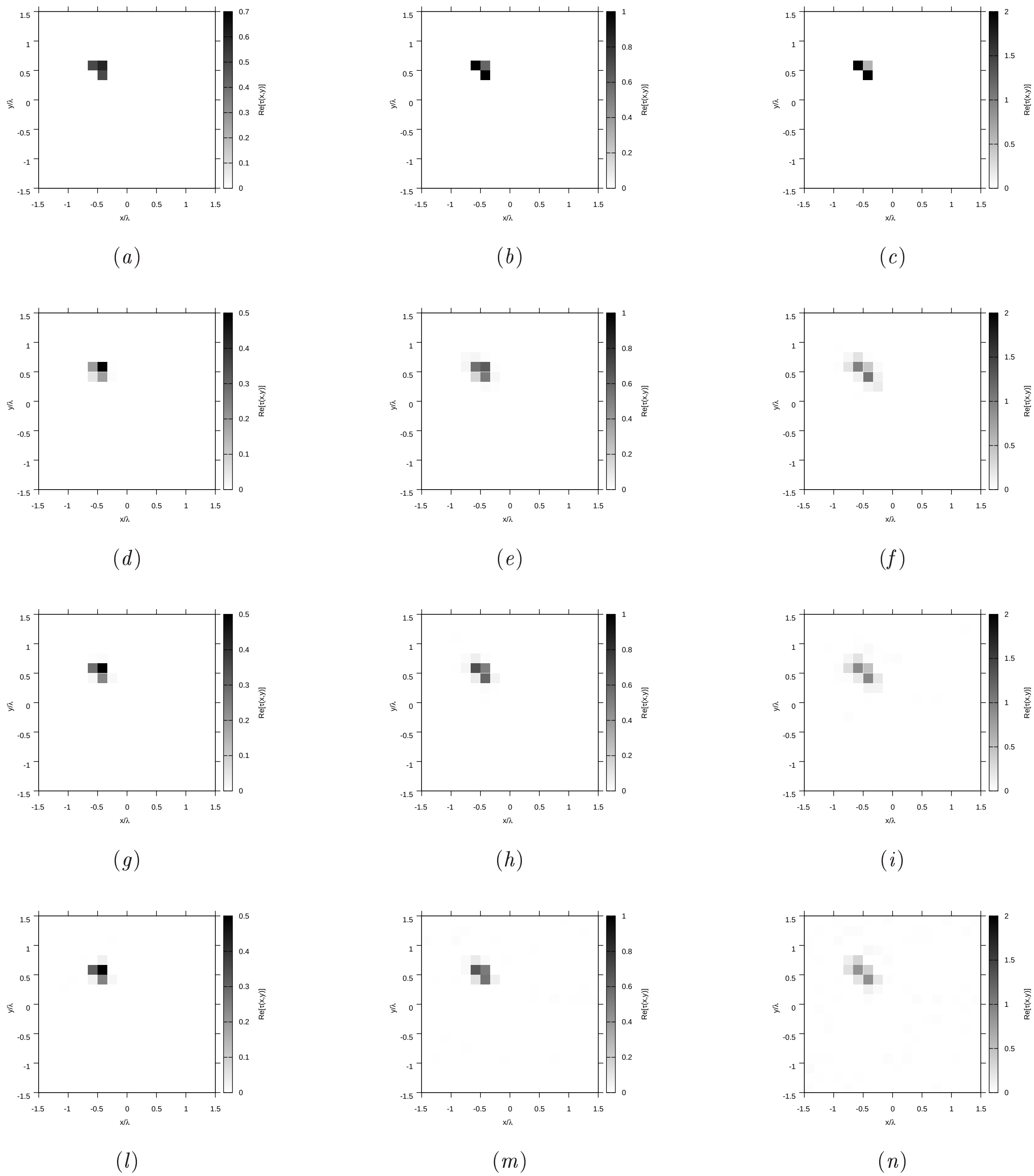

Figure 7. Actual object $(a)(b)(c)$ and BCS reconstructed object with $(d)(g)(l)$ $\varepsilon_r = 1.5$, $(e)(h)(m)$ $\varepsilon_r = 2.0$, and $(f)(i)(n)$ $\varepsilon_r = 3.0$, for $(d)(e)(f)$ Noiseless case, $(g)(h)(i)$ $SNR = 10$ [dB] and $(l)(m)(n)$ $SNR = 5$ [dB].

RESULTS: Inhomogeneous L-Shaped Cylinder - Error Figures - Comparison Born/Rytov Approximation

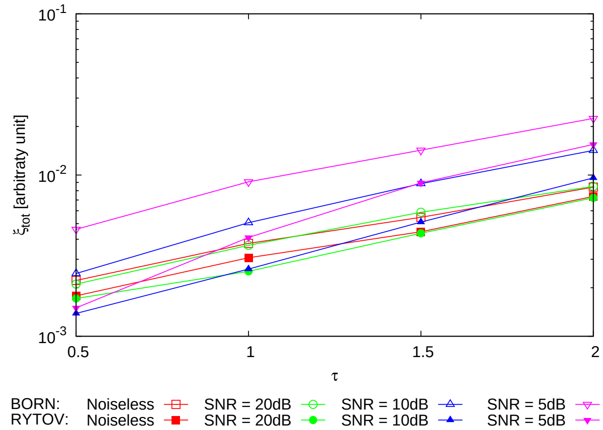

(a)

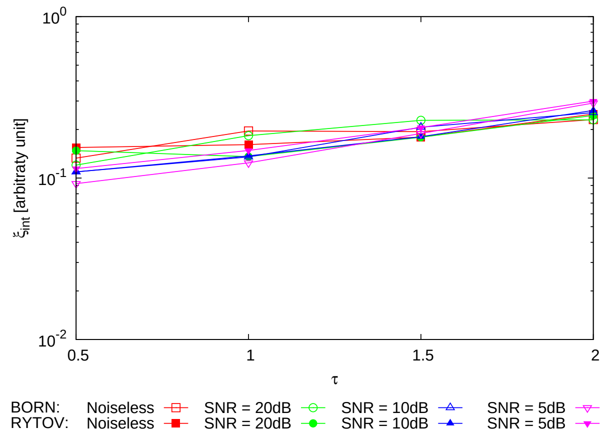

(b)

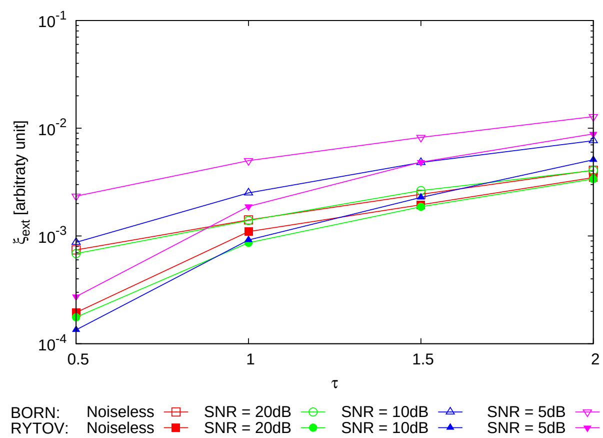

(c)

Figure 8. Behaviour of error figures as a function of ε_r, for different SNR values: (a) total error ξ_{tot}, (b) internal error ξ_{int}, (c) external error ξ_{ext}.

1.5 TEST CASE: Two Square Cylinders on the Diagonal

Goal: evaluate the the performances of BCS

- Number of Views: V
- Number of Measurements: M
- Number of Cells for the Inversion: N
- Number of Cells for the Direct solver: D
- Side of the investigation domain: L

Test Case Description

Direct solver:

- Square domain divided in $\sqrt{D} \times \sqrt{D}$ cells
- Domain side: $L = 3\lambda$
- $D = 1296$ (discretization for the direct solver: $< \lambda/10$)

Investigation domain:

- Square domain divided in $\sqrt{N} \times \sqrt{N}$ cells
- $L = 3\lambda$
- $N = 324$

Measurement domain:

- Measurement points taken on a circle of radius $\rho = 3\lambda$
- Full-aspect measurements
- $M \approx 2ka \rightarrow M = 27$

Sources:

- Plane waves
- $V \approx 2ka \rightarrow V = 27$
- Amplitude $A = 1$
- Frequency: 300 MHz ($\lambda = 1$)

Object:

- Two square cylinders of side $\frac{\lambda}{6} = 0.16667$ at a distance Δx, Δy from each other
- $\varepsilon_r \in \{1.5, 2.0, 2.5, 3.0\}$
- $\sigma = 0$ [S/m]

BCS parameters:

- Initial estimate of the noise: $n_0 = 8.0 \times 10^{-3}$
- Convergenze parameter: $\tau = 1.0 \times 10^{-8}$

Resolution Analysis:

- $\Delta x = \Delta y = \{k\lambda/10,\, k = 0, ..., 14\}$

RESULTS: Two Square Cylinders on the Diagonal - $\varepsilon_r = 1.5$

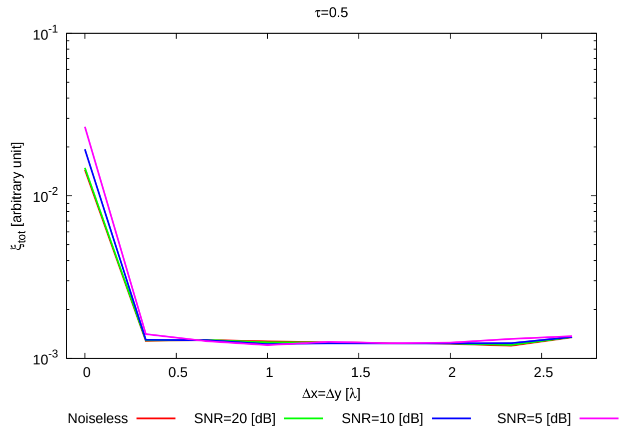

(a)

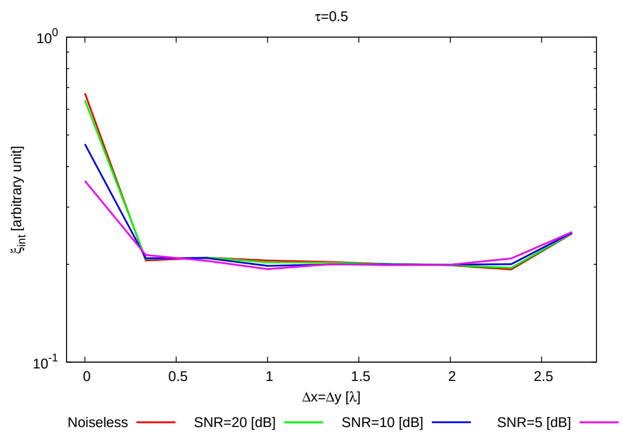

(b)

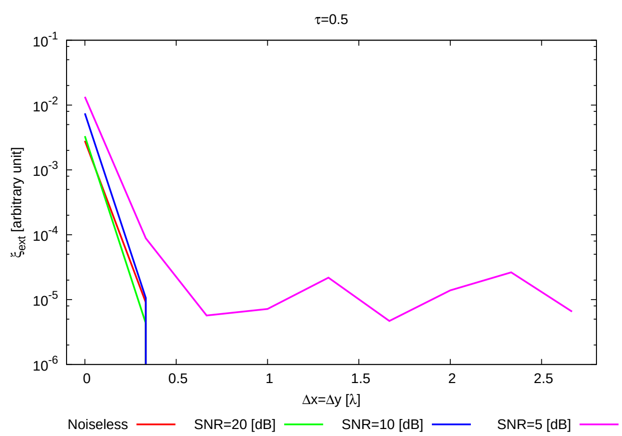

(c)

Figure 9. *Resolution analysis* - Behaviour of error figures as a function of $\Delta x = \Delta y$ for different SNR values: (a) total error ξ_{tot}, (b) internal error ξ_{int}, (c) external error ξ_{ext}.

RESULTS: Two Square Cylinders on the Diagonal - $\varepsilon_r = 2.0$

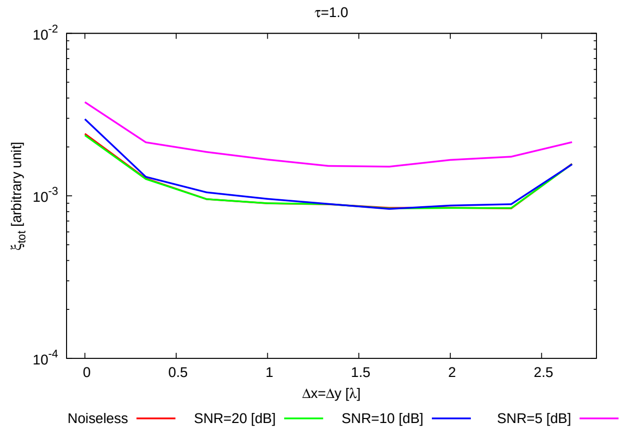

(a)

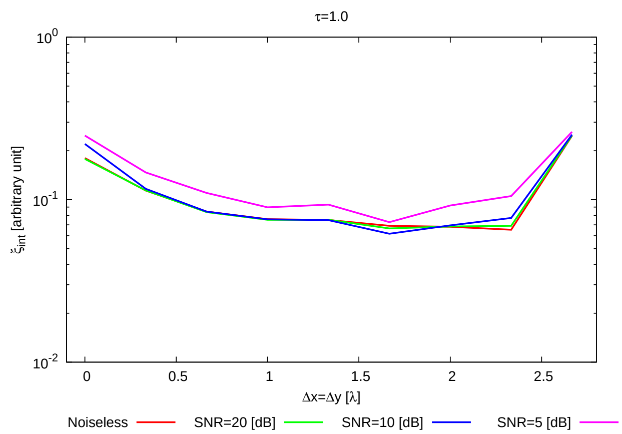

(b)

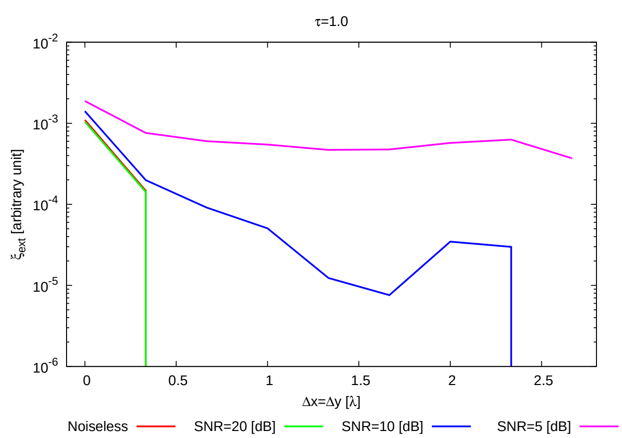

(c)

Figure 19. *Resolution analysis* - Behaviour of error figures as a function of $\Delta x = \Delta y$ for different SNR values: (a) total error ξ_{tot}, (b) internal error ξ_{int}, (c) external error ξ_{ext}.

RESULTS: Two Square Cylinders on the Diagonal - $\varepsilon_r = 2.5$

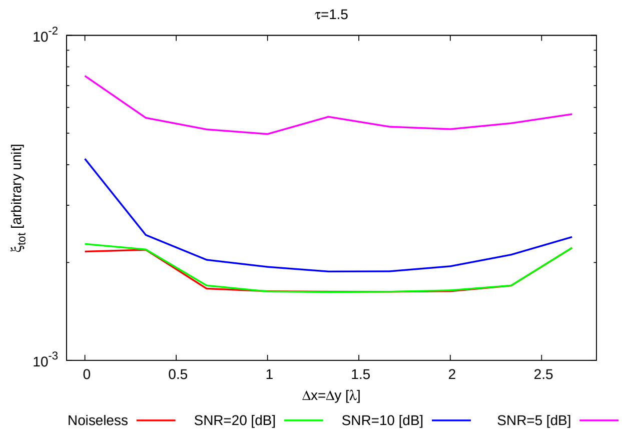

(a)

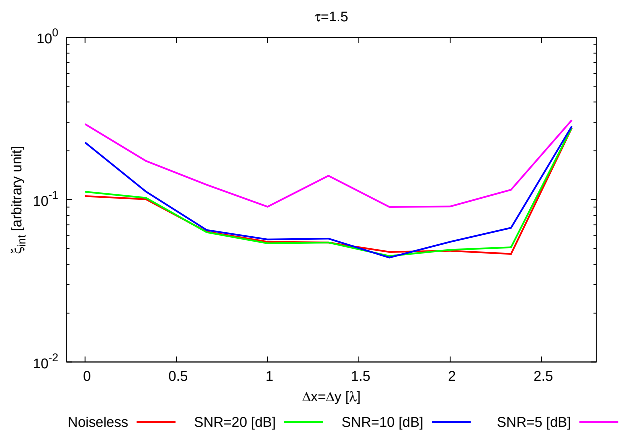

(b)

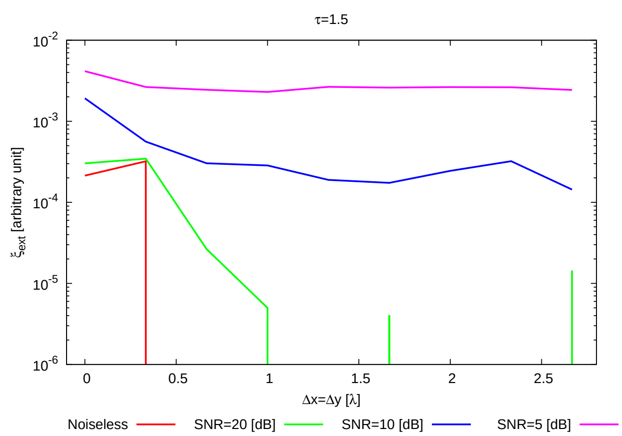

(c)

Figure 10. *Resolution analysis* - Behaviour of error figures as a function of $\Delta x = \Delta y$ for different SNR values: (a) total error ξ_{tot}, (b) internal error ξ_{int}, (c) external error ξ_{ext}.

RESULTS: Two Square Cylinders on the Diagonal - $\varepsilon_r = 3.0$

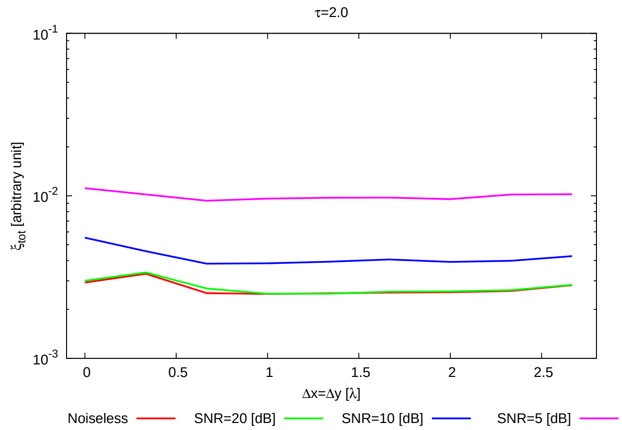

(a)

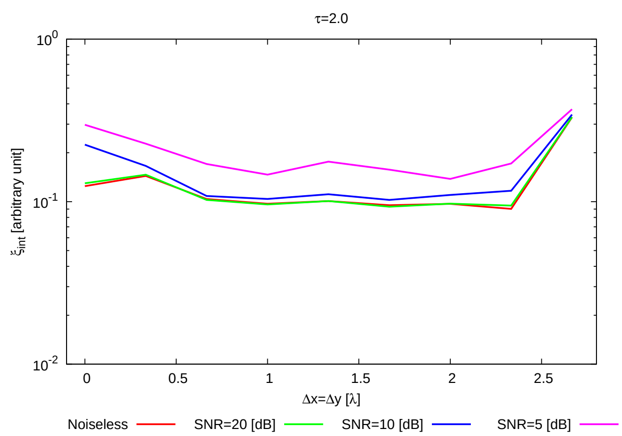

(b)

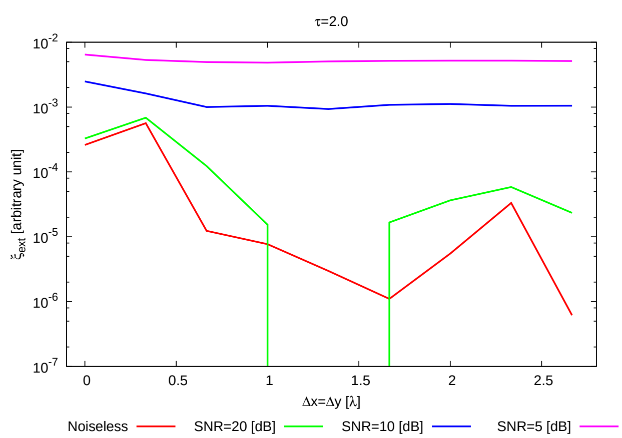

(c)

Figure 11. *Resolution analysis* - Behaviour of error figures as a function of $\Delta x = \Delta y$ for different SNR values: (a) total error ξ_{tot}, (b) internal error ξ_{int}, (c) external error ξ_{ext}.

References

[1] L. Poli, G. Oliveri, and A. Massa, "Imaging sparse metallic cylinders through a Local Shape Function Bayesian Compressive Sensing approach," Journal of Optical Society of America A, vol. 30, no. 6, pp. 1261-1272, 2013.

[2] F. Viani, L. Poli, G. Oliveri, F. Robol, and A. Massa, "Sparse scatterers imaging through approximated multitask compressive sensing strategies," Microwave Opt. Technol. Lett., vol. 55, no. 7, pp. 1553-1558, Jul. 2013.

[3] L. Poli, G. Oliveri, P. Rocca, and A. Massa, "Bayesian compressive sensing approaches for the reconstruction of two-dimensional sparse scatterers under TE illumination," IEEE Trans. Geosci. Remote Sensing, vol. 51, no. 5, pp. 2920-2936, May. 2013.

[4] L. Poli, G. Oliveri, and A. Massa, "Microwave imaging within the first-order Born approximation by means of the contrast-field Bayesian compressive sensing," IEEE Trans. Antennas Propag., vol. 60, no. 6, pp. 2865-2879, Jun. 2012.

[5] G. Oliveri, P. Rocca, and A. Massa, "A bayesian compressive sampling-based inversion for imaging sparse scatterers," IEEE Trans. Geosci. Remote Sensing, vol. 49, no. 10, pp. 3993-4006, Oct. 2011.

[6] G. Oliveri, L. Poli, P. Rocca, and A. Massa, "Bayesian compressive optical imaging within the Rytov approximation," Optics Letters, vol. 37, no. 10, pp. 1760-1762, 2012.

[7] L. Poli, G. Oliveri, F. Viani, and A. Massa, "MT-BCS-based microwave imaging approach through minimum-norm current expansion," IEEE Trans. Antennas Propag., in press. doi:10.1109/TAP.2013.2265254

[8] G. Oliveri and A. Massa, "Bayesian compressive sampling for pattern synthesis with maximally sparse non-uniform linear arrays," IEEE Trans. Antennas Propag., vol. 59, no. 2, pp. 467-481, Feb. 2011.

[9] G. Oliveri, M. Carlin, and A. Massa, "Complex-weight sparse linear array synthesis by Bayesian Compressive Sampling," IEEE Trans. Antennas Propag., vol. 60, no. 5, pp. 2309-2326, May 2012.

[10] G. Oliveri, P. Rocca, and A. Massa, "Reliable Diagnosis of Large Linear Arrays - A Bayesian Compressive Sensing Approach," IEEE Trans. Antennas Propag., vol. 60, no. 10, pp. 4627-4636, Oct. 2012.

[11] F. Viani, G. Oliveri, and A. Massa, "Compressive sensing pattern matching techniques for synthesizing planar sparse arrays" IEEE Trans. Antennas Propag., in press. doi:10.1109/TAP.2013.2267195

[12] M. Carlin, P. Rocca, G. Oliveri, F. Viani, and A. Massa, "Directions-of-Arrival Estimation through Bayesian Compressive Sensing strategies," IEEE Trans. Antennas Propag., in press.

[13] M. Carlin, P. Rocca, "A Bayesian compressive sensing strategy for direction-of-arrival estimation," 6th European Conference on Antennas Propag. (EuCAP 2012), Prague, Czech Republic, pp. 1508-1509, 26-30 Mar. 2012.

[14] M. Carlin, P. Rocca, G. Oliveri, and A. Massa, "Bayesian compressive sensing as applied to directions-of-arrival estimation in planar arraysâ" Journal of Electrical and Computer Engineering, Special Issue on "Advances in Radar Technologiesâ" in press.

[15] M. Donelli, D. Franceschini, P. Rocca, and A. Massa, "Three-dimensional microwave imaging problems solved through an efficient multi-scaling particle swarm optimization," IEEE Trans. Geosci. Remote Sensing, vol. 47, no. 5, pp. 1467-1481, May 2009.

[16] M. Benedetti, G. Franceschini, R. Azaro, and A. Massa, "A numerical assessment of the reconstruction effectiveness of the integrated GA-based multicrack strategy," IEEE Antennas Wireless Propag. Lett., vol. 6, pp. 271-274, 2007.

[17] P. Rocca, M. Carlin, G. Oliveri, and A. Massa, "Interval analysis as applied to inverse scattering," IEEE International Symposium on Antennas Propag. (APS/URSI 2013), Chicago, Illinois, USA, Jul. 8-14, 2012.

[18] L. Manica, P. Rocca, M. Salucci, M. Carlin, and A. Massa, "Scattering data inversion through interval analysis under Rytov approximation," 7th European Conference on Antennas Propag. (EuCAP 2013), Gothenburg, Sweden, Apr. 8-12, 2013.

[19] P. Rocca, M. Carlin, and A. Massa, "Imaging weak scatterers by means of an innovative inverse scattering technique based on the interval analysis," 6th European Conference on Antennas Propag. (EuCAP 2012), Prague, Czech Republic, Mar. 26-30, 2012.

[20] S. C. Hagness, E. C. Fear, and A. Massa, "Guest Editorial: Special Cluster on Microwave Medical Imaging", IEEE Antennas Wireless Propag. Lett., vol. 11, pp. 1592-1597, 2012.

[21] G. Oliveri, Y. Zhong, X. Chen, and A. Massa, "Multi-resolution subspace-based optimization method for inverse scattering," Journal of Optical Society of America A, vol. 28, no. 10, pp. 2057-2069, Oct. 2011.

[22] A. Randazzo, G. Oliveri, A. Massa, and M. Pastorino, "Electromagnetic inversion with the multiscaling inexact-Newton method - Experimental validation," Microwave Opt. Technol. Lett., vol. 53, no. 12, pp. 2834-2838, Dec. 2011.

[23] G. Oliveri, L. Lizzi, M. Pastorino, and A. Massa, "A nested multi-scaling inexact-Newton iterative approach for microwave imaging," IEEE Trans. Antennas Propag., vol. 60, no. 2, pp. 971-983, Feb. 2012.

[24] G. Oliveri, A. Randazzo, M. Pastorino, and A. Massa, "Electromagnetic imaging within the contrast-source formulation by means of the multiscaling inexact Newton method," Journal of Optical Society of America A, vol. 29, no. 6, pp. 945-958, 2012.

[25] M. Benedetti, D. Lesselier, M. Lambert, and A. Massa, "Multiple shapes reconstruction by means of multi-region level sets," IEEE Trans. Geosci. Remote Sensing, vol. 48, no. 5, pp. 2330-2342, May 2010.

[26] M. Benedetti, D. Lesselier, M. Lambert, and A. Massa, "A multi-resolution technique based on shape optimization for the reconstruction of homogeneous dielectric objects," Inverse Problems, vol. 25, no. 1, pp. 1-26, Jan. 2009.